Synthesis, Structure, Magnetic Properties, and XANES Spectra of Reduced Niobate $RbNa_xCa_2Nb_3O_{10}$

Song-Ho Byeon,*,† Hee Jin Kim,† Dong-Kuk Kim,‡ and Nam Hwi Hur§

College of Environment and Applied Chemistry, Institute of Natural Sciences, Kyung Hee University, Kyung Ki 449-701, Korea, Department of Chemistry, College of Natural Sciences, Kyungpook National University, Taegu 702-701, Korea, and Center for CMR Materials, KRISS, Yusong P.O. Box 102, Taejon 305-600, Korea

Received March 14, 2002. Revised Manuscript Received September 16, 2002

Reduced layered niobate $RbNa_xCa_2Nb_3O_{10}$ was synthesized via the reaction of $RbCa_2Nb_3O_{10}$ with sodium vapor at 500 °C. The structure has been refined from X-ray powder diffraction data, revealing that this black compound crystallizes in the space group $P4_2/ncm$ with $a =$ 5.4790(3) Å, $c = 28.8264(9)$ Å, and $Z = 4$. The NbO_6 octahedra are slightly tilted, and the interlayer geometry between the $Ca_2Nb_3O_8$ units is similar to those of $Rb_2La_2Nb_3O_{10}$ and β-$NaCa_2Nb_3O_{10}$. Magnetization measurements show no indication of superconductivity down to 4 K and instead exhibit a typical paramagnetic behavior. The influence of reductive sodium insertion on the electronic structure is discussed on the basis of Nb K-edge and O K-edge XANES spectra of $RbNa_xCa_2Nb_3O_{10}$. In addition, we report the crystal structure of another layered niobate, β-$NaCa_2Nb_3O_{10}$, which was synthesized by the ion-exchange reaction of $RbCa_2Nb_3O_{10}$ in molten $NaNO_3$ at 340 °C. Powder neutron diffraction reveals that the white compound also adopts a tetragonal symmetry (space group $P4_2/ncm$) with cell constants $a =$ 5.4731(2) Å, $c = 29.0138(9)$ Å, and $Z = 4$. The Na atoms occupy the 5-coordinated sites in the interlayer space of β-$NaCa_2Nb_3O_{10}$.

Introduction

A number of investigations have been performed to synthesize perovskite-related compounds and to understand their structural characteristics.[1−4] Some families of layered perovskite materials exhibit diverse interesting physical and chemical phenomena such as ion-exchange and intercalation reactions, high ionic conductivity, photocatalysis, superconductivity, and magnetoresistivity.[5−10] Recently, several new members have been added to the growing list of layered perovskite families.[11−15]

Layered niobate $ACa_2Nb_3O_{10}$ (A = alkali metals) is one of the $n = 3$ members of the Dion−Jacobson (DJ) series having the general formula $A[A'_{n-1}B_nO_{3n+1}]$.[3,16] Interestingly, the coordinating geometry of the interlayer A atom is heavily dependent upon its size. A large cation like Cs or Rb occupies a distorted cubic site,[16] but a small Li ion prefers to fill the tetrahedral site between adjacent perovskite layers.[17] On the other hand, the K atom that can be considered as the medium size possesses a trigonal prismatic site.[18] The occupation of the trigonal prismatic or tetrahedral site leads to a doubling of the *c* axis. This versatile coordinating behavior of the A cation prompted us to investigate the addition of the small Na ion into the $RbCa_2Nb_3O_{10}$ compound, which enables us to make the new reduced niobate. Our expectation is based on the fact that the intercalation reaction by an alkali metal is an effective

* To whom correspondence should be addressed.
† Kyung Hee University.
‡ Kyungpook National University.
§ KRISS.

(1) Aurivillius, B. *Ark. Kemi.* **1949**, *1*, 463; **1950**, *2*, 519.
(2) Ruddlesden, S. N.; Popper, P. *Acta Crystallogr.* **1957**, *10*, 538; **1958**, *11*, 54.
(3) (a) Dion, M.; Ganne, M.; Tournoux, M. *Mater. Res. Bull.* **1981**, *16*, 1429. (b) Jacobson, A. J.; Johnson, J. W.; Lewandowski, J. T. *Inorg. Chem.* **1985**, *24*, 3727.
(4) (a) Gopalakrishnan, J.; Bhat, V.; Raveau, B. *Mater. Res. Bull.* **1987**, *22*, 413. (b) Gopalakrishnan, J.; Bhat, V. *Inorg. Chem.* **1987**, *26*, 4299. (c) Subramanian, M. A.; Gopalakrishnan, J.; Sleight, A. W. *Mater. Res. Bull.* **1988**, *23*, 837.
(5) (a) Domen, K.; Yoshimura, J.; Sekine, T.; Tanaka, A.; Onishi, T. *Catal. Lett.* **1990**, *4*, 339. (b) Ikeda, S.; Hara, M.; Kondo, J. N.; Domen, K.; Takahashi, H.; Okubo, T.; Kakihana, M. *Chem. Mater.* **1998**, *10*, 72.
(6) (a) Uma, S.; Raju, A. R.; Gopalakrishnan, J. *J. Mater. Chem.* **1993**, *3*, 709. (b) Uma, S.; Gopalakrishnan, J. *Chem. Mater.* **1994**, *6*, 907.
(7) (a) Sato, M.; Watanabe, J.; Uematsu, K. *J. Solid State Chem.* **1993**, *107*, 460. (b) Toda, K.; Sato, M. *J. Mater. Chem.* **1996**, *6*, 1067.
(8) (a) Byeon, S.-H.; Park, K.; Itoh, M. *J. Solid State Chem.* **1996**, *121*, 430. (b) Byeon, S.-H.; Yoon, J.-J.; Lee, S.-O. *J. Solid State Chem.* **1996**, *127*, 119.
(9) Moritomo, Y.; Asamitsu, A.; Kuwahara, H.; Tokura, Y. *Nature* **1996**, *380*, 141.
(10) Seshadri, R.; Martin, C.; Herien, M.; Raveau, B.; Rao, C. N. R. *Chem. Mater.* **1997**, *9*, 270.
(11) McIntyre, R. A.; Falster, A. U.; Li, S.; Simmons, W. B.; O'Connor, C. J.; Wiley, J. B. *J. Am. Chem. Soc.* **1998**, *120*, 217.
(12) Toda, K.; Takahashi, M.; Teranishi, T.; Ye, Z.; Sato, M.; Hinatsu, Y. *J. Mater. Chem.* **1999**, *9*, 799.
(13) Floros, N.; Michel, C.; Hervieu, M.; Raveau, B. *J. Mater. Chem.* **1999**, *9*, 3101.
(14) (a) Crosnier-Lopez, M. P.; Duroy, H.; Fourquet, J. L. *Mater. Res. Bull.* **1999**, *34*, 179. (b) Bhuvanesh, N. S.; Crosnier-Lopez, M. P.; Bohnke, O.; Emery, J.; Fourquet, J. L. *Chem. Mater.* **1999**, *11*, 634.
(15) Hyeon, K.-A.; Byeon, S.-H. *Chem. Mater.* **2000**, *11*, 352.
(16) (a) Dion, M.; Ganne, M.; Tournoux, M.; Ravez, J. *Rev. Chim. Miner.* **1984**, *21*, 92. (b) Dion, M.; Ganne, M.; Tournoux, M. *Rev. Chim. Miner.* **1986**, *23*, 61.
(17) Toda, K.; Teranishi, T.; Ye, Z.-G.; Sato, M.; Hinatsu, Y. *Mater. Res. Bull.* **1999**, *34*, 971.
(18) Fukuoka, H.; Isami, T.; Yamanaka, S. *J. Solid State Chem.* **2000**, *151*, 40.

10.1021/cm020270b CCC: $25.00
Published on Web 12/20/2002

topotactic method for the low-temperature synthesis of layered oxides with mixed valence.[19−24] The Na insertion into the interlayer site would thus not only provide a new compound with a different interlayer coordinating mode but also render a new opportunity to discover unique physical phenomena due to charge carriers stemmed from the Nb^{IV} (d^1) ion. In fact, the Li intercalation into $KCa_2Nb_3O_{10}$ has made the parent insulating compound superconducting while no superconductivity is found in Li-doped compound $KLaNb_2O_7$.[25] The central NbO_6 octahedral layer, which is only weakly affected by the alkali metal, is likely to be responsible for the superconducting behavior in the former compound. This strongly suggests that the physical property of the layered niobate is sensitive to the nature of the coordinating geometry of the A cation.

In this paper, we mainly describe the synthesis, structure, and magnetic properties of the Na-inserted compound $RbNa_xCa_2Nb_3O_{10}$. It is found that Nb^V is partially reduced, as confirmed by Nb K-edge and O K-edge XANES spectra, but the black compound does not show any indication of superconductivity. The structure of $RbNa_xCa_2Nb_3O_{10}$, especially the coordination of the Rb and Na ions, distinguishes it from other Dion−Jacobson compounds. In addition, the structure of β-$NaCa_2Nb_3O_{10}$ was also investigated in terms of neutron diffraction, showing that the Na coordination is quite analogous to that of $RbNa_xCa_2Nb_3O_{10}$.

Experimental Section

Synthesis. The parent layered niobate, $RbCa_2Nb_3O_{10}$, was prepared by conventional solid state reaction.[3a] The mixture of Rb_2CO_3, $CaCO_3$, and Nb_2O_5 was heated in air at 1150 °C for 12 h with intermittent grindings, in which about 30 mol % of excess Rb_2CO_3 was added to compensate for the loss of volatile rubidium. After the reaction, the remaining rubidium component was washed out with distilled water and dried at 120 °C. Special care has to be taken with the synthesis of reduced niobate $RbNa_xCa_2Nb_3O_{10}$ because of its extreme sensitivity to air. All the operations were thus handled in an argon-filled drybox. A thin quartz tube that contains an excess amount of sodium was placed inside a thick quartz tube along with $RbCa_2Nb_3O_{10}$, which was then sealed under vacuum. The oxide turned from white to black during heat treatment of the sample at 500 °C for 5 days. Heating the sample tube in a weak temperature gradient after the reaction eliminated excess sodium adsorbed on the surface of sample particles. β-$NaCa_2Nb_3O_{10}$ was prepared by the ion-exchange reaction of $RbCa_2Nb_3O_{10}$ with the molten $NaNO_3$ salt at 340 °C for 4 days. The mixture was replaced once in between. After the exchange reaction, excess $NaNO_3$ in the solid product was washed out with hot water and dried at 120 °C. The hydrated form of $NaCa_2Nb_3O_{10}$ was obtained when the solid product was dried at room temperature after the washing. The β-$NaCa_2Nb_3O_{10}$ compound was converted to the α-form upon heating at around 650 °C.

Characterization. The stoichiometric compositions of α- and β-$NaCa_2Nb_3O_{10}$ were confirmed by the elemental analysis of sodium using ion chromatography (IC). About 10 mg of the sample was dissolved in about 10 mL of mixed solution of HF and HNO_3. Elemental analysis using the energy-dispersive X-ray emission (EDX) technique also gave the stoichiometric compositions within experimental errors. The temperature higher than 380 °C was required for a complete dehydration of $NaCa_2Nb_3O_{10}{\cdot}xH_2O$, and the amount ($x$) of intercalated water was determined by the thermal gravimetric analysis. A weight loss from 80 °C up to ∼380 °C reached to ∼2 H_2O per formula unit.

Structure Analysis. All the compounds synthesized in this work were initially characterized by the X-ray diffraction method. X-ray diffraction data were recorded on a rotating anode installed diffractometer with an X-ray source of 40 kV, 300 mA. In particular, scans for the reduced niobate $RbNa_xCa_2Nb_3O_{10}$ were taken from $2\theta = 10°$ to $2\theta = 70°$ with a step size of 0.02° within 4 min owing to its high air-sensitivity. Neutron diffraction data of β-$NaCa_2Nb_3O_{10}$ were measured over the 2θ range of 10° to 160° with a step size of 0.05° on a high-resolution powder diffractometer at HANARO Center in KAERI, where a neutron source with $\lambda = 1.8348$ Å supplied by Ge(331) single-crystal monochromator was used. The ground powders were loaded in a vanadium can. The diffraction data were analyzed by profile analysis based on the Rietan program.[26]

Magnetic Susceptibility Measurement. The magnetic measurements for $RbNa_xCa_2Nb_3O_{10}$ were carried out in the temperature range from 5 to 40 K in an applied magnetic field of 100 G using a Quantum Design MPMS-5 SQUID magnetometer. The sample to be measured was weighed and placed into a NMR tube (diameter = 5 mm) in an argon-filled drybox, which was then sealed under vacuum.

X-ray Absorption Near Edge Spectroscopy (XANES). The soft X-ray absorption measurements for O K-edge spectra were performed at the U7 beamline at Pohang Light Source (PLS). The spectra were recorded in the total-electron yields from sample current and normalized by photon current from gold grid with 90% transmission. The energy in spectra was calibrated using Au 4f photoemission line and L_3-edges in pure d-metals. Nb K-edge spectra were measured at the 3C beam line of PLS in the transmission mode. The energy calibration was carried out by niobium foil simultaneously measured with the specimens. Both O K-edge and Nb K-edge spectra were normalized after background correction of the pre-edge region.

Results and Discussion

Synthesis and Characterization. The synthesis of a Na-inserted $RbNa_xCa_2Nb_3O_{10}$ is heavily dependent on the reaction temperature because the sodium is very volatile in an evacuated quartz tube. In an attempt to control the amount of sodium inserted into $RbCa_2Nb_3O_{10}$, several additional experiments have been carried out at different temperatures and partial pressures of sodium vapor. Only when the reaction takes place at 500 °C does the product show a well crystallized single phase. While lower temperatures (400−480 °C) required much longer reaction time (>15 days) and resulted in a poor crystallinity, higher temperatures (>550 °C) led to sodium loss and reformation of $RbCa_2Nb_3O_{10}$. Unfortunately, the amount (x) of inserted sodium content in $RbNa_xCa_2Nb_3O_{10}$ could not be precisely determined because a weak temperature gradient method eliminates only a partial amount of sodium adsorbed on the surface of sample. Several repetitions of qualitative analyses using IC and EDX methods always gave a

(19) Nadiri, A.; Le Flem, G.; Delmas, C. *J. Solid State Chem.* **1988**, *73*, 338.
(20) Hagenmuller, P.; Delmas, C. *Mater. Res. Soc. Symp. Proc.* **1991**, *210*, 323.
(21) Jones, R.; McKinnon, W. R. *Solid State Ionics* **1991**, *45*, 173.
(22) Gomez-Romero, P.; Palacin, M. R.; Casan, N.; Fuertes, A. *Solid State Ionics* **1993**, *63−65*, 424.
(23) Armstrong, A. R.; Anderson, P. A. *Inorg. Chem.* **1994**, *33*, 4366.
(24) Bohnke, C.; Bohnke, O.; Fourquet, J. L. *J. Electrochem. Soc.* **1997**, *144*, 1151.
(25) (a) Takano, Y.; Taketomi, H.; Tsurumi, H.; S.; Yamadaya, T.; Mori, N. *Physica B* **1997**, *237*, 68. (b) Takano, Y.; Takayanagi, S.; Ogawa, S.; Yamadaya, T.; Mori, N. *Solid State Commun.* **1997**, *103*, 215.
(26) Izumi. F.; Murata, H.; Watanabe, N. *J. Appl. Crystallogr.* **1987**, *20*, 411.

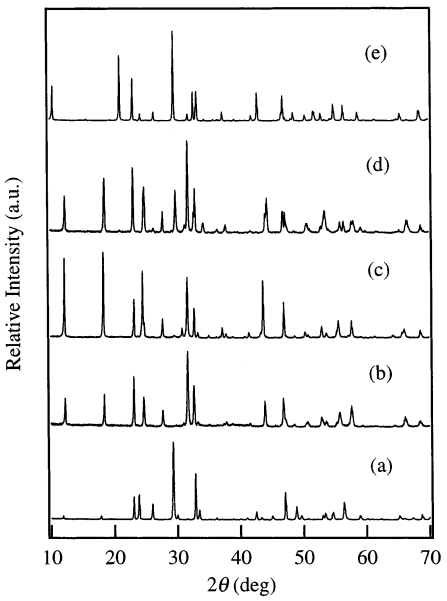

Figure 1. X-ray diffraction patterns of (a) $RbCa_2Nb_3O_{10}$, (b) $RbNa_xCa_2Nb_3O_{10}$, (c) β-$NaCa_2Nb_3O_{10}$, (d) α-$NaCa_2Nb_3O_{10}$, and (e) $NaCa_2Nb_3O_{10}\cdot 2H_2O$.

result of $x > 1.5$ for $RbNa_xCa_2Nb_3O_{10}$, which largely exceeds an insertion capacity. When a complete elimination of adsorbed sodium was tried in a strong temperature gradient, a loss of inserted sodium resulted in a formation of white $RbCa_2Nb_3O_{10}$.

The X-ray diffraction patterns of all the compounds synthesized in this work are compared in Figure 1. There are clear distinctions among the diffraction patterns, which strongly depend on the nature of alkali metal interlayer spaces. The cell parameters of $RbCa_2Nb_3O_{10}$ and α- and β-$NaCa_2Nb_3O_{10}$ and hydrated forms of $NaCa_2Nb_3O_{10}$, which adopt the tetragonal symmetry, were in good agreement with those previously reported by Dion et al.[3a] It is noteworthy that the *c* parameter (16.832(1) Å) of $NaCa_2Nb_3O_{10}\cdot 2H_2O$ in this work was different from that ($c = 15.137(8)$ Å) of $NaCa_2Nb_3O_{10}\cdot H_2O$, indicating that a hydration degree can be quite different depending on the partial pressure of water. Moreover, we found a transformation from β- to α-$NaCa_2Nb_3O_{10}$ at around 650 °C, which is much lower than the reported temperature (900 °C). The α-form was collapsed above 800 °C.

It was difficult to expose $RbNa_xCa_2Nb_3O_{10}$ to the neutron beam for a long time because of its extreme air-sensitivity. Intensity data for the structure determination of $RbNa_xCa_2Nb_3O_{10}$ were therefore obtained by the X-ray diffraction technique as noted in the Experimental Section.

Structure Refinement. The *c* parameter of $RbNa_xCa_2Nb_3O_{10}$ was calculated to be 28.83 Å by the least-squares method, suggesting that the *c* axis is doubled by a relative displacement of adjacent perovskite slabs toward a staggered conformation. This doubling feature is quite analogous to that found in β-$NaCa_2Nb_3O_{10}$. Therefore, we first refined the powder neutron diffraction data of β-$NaCa_2Nb_3O_{10}$ to obtain structural information for the refinement of $RbNa_xCa_2Nb_3O_{10}$. It has been reported that $NaCa_2Nb_3O_{10}$ crystallizes in the α- and β-forms depending on the temperature.[3] According to a structure model for the low temperature β-form, the Na atoms are statistically distributed at one-half of the Na positions found in the Ruddlesden−Popper (RP) type $Na_2La_2Ti_3O_{10}$.[27] On the other hand, it is expected in a model for the high temperature α-form that the interlayer space is composed of tetrahedral sites, one-half of which are occupied by the Na atoms. To the best of our knowledge, however, such structural models have not yet been crystallographically confirmed.

It has been reported that the Ta analogue, $NaCa_2Ta_3O_{10}$, crystallizes in the space group $I4/mmm$.[12] Initial attempts to refine the structure of β-$NaCa_2Nb_3O_{10}$ based on the same space group ($a \sim 3.87$ Å and $c \sim 29.0$ Å) gave poor results, and there were a number of additional peaks that could not be fitted with this simple model. Although no clear reflection condition was observed because of substantial peak overlap in the neutron diffraction pattern, none of the possible space groups consistent with the body centered structural model gave satisfactory results. The orthorhombic space group *Cmcm*, which is well adopted to $KCa_2Nb_3O_{10}$,[17] was then tested with possible shifts of the sodium position. However, this orthorhombic model also yielded a poor fit to the additional reflections. Use of a model-independent fit led to the identification of a $\sqrt{2} \times \sqrt{2} \times 1$ supercell. Accordingly, the structure refinement of β-$NaCa_2Nb_3O_{10}$ was tried again using initial atomic positions (space group $P4_2/ncm$) of $Li_2La_{1.78}(Nb_{0.66}Ti_{2.34})O_{10}$ which shows a similar supercell.[28] Considering that the sodium atoms would be statistically distributed at one-half of the lithium positions 4b ($^3/_4$, $^1/_4$, $^1/_4$) and 4e ($^3/_4$, $^3/_4$, *z*) in this structure, the occupancy factors of sodium atoms were kept at 0.5 during refinement. Unfortunately, this refinement gave poor reliability factors and large or negative isotropic temperature factors. When the position of sodium atom is shifted to 8i (*x*, *x*, *z*) rather than 4b and 4e, the refinement converged rapidly in the space group $P4_2/ncm$ to agreeable profile fit parameters.

A number of structural models, which have been reported for DJ- or RP-phases in the literature, were attempted to fit the diffraction data of $RbNa_xCa_2Nb_3O_{10}$. We found that an adoption of the tetragonal space group $P4_2/ncm$ enables the most satisfactory fitting. As can be seen in Figure 1b,c, the powder X-ray diffraction patterns of β-$NaCa_2Nb_3O_{10}$ and $RbNa_xCa_2Nb_3O_{10}$ are analogous to each other. Therefore, the structure data for β-$NaCa_2Nb_3O_{10}$ were used to provide the initial atom positions within the unit cell of $RbNa_xCa_2Nb_3O_{10}$. The rubidium atoms were then located at 8i sites with half occupancy. Allowing the occupancy of sodium atoms to be refined, the reliability *R* factors decreased rapidly. Isotropic thermal parameters of rubidium, sodium, and oxygen atoms were fixed to 1.0 before final stage of refinement.

The observed, calculated, and difference profiles for β-$NaCa_2Nb_3O_{10}$ and $RbNa_xCa_2Nb_3O_{10}$ are plotted in Figures 2 and 3. Selected crystallographic data and final reliability factors for both phases are listed in Tables 1 and 2. The *c* parameter of $RbNa_xCa_2Nb_3O_{10}$ is slightly smaller than that of β-$NaCa_2Nb_3O_{10}$, indicating that the

(27) Toda, K.; Kameo, Y.; Fujimoto, M.; Sato, M. *J. Ceram. Soc. Jpn.* **1994**, *102*, 737.
(28) Bhuvanesh, N. S.; Crosnier-Lopez, M. P.; Duroy, H.; Fourquet, J. L. *J. Mater. Chem.* **1999**, *9*, 3093.

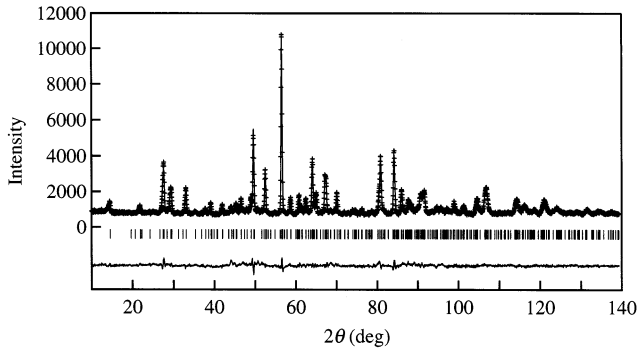

Figure 2. Calculated (solid line), experimental (dotted line), and difference (solid lines on the bottom) neutron powder diffraction patterns of β-$NaCa_2Nb_3O_{10}$.

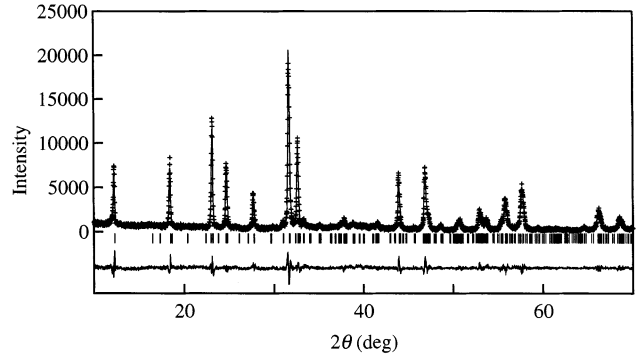

Figure 3. Calculated (solid line), experimental (dotted line), and difference (solid lines on the bottom) X-ray powder diffraction patterns of $RbNa_xCa_2Nb_3O_{10}$.

Table 1. Crystallographic Data of β-$NaCa_2Nb_3O_{10}$ and $RbNa_xCa_2Nb_3O_{10}$

	β-$NaCa_2Nb_3O_{10}$[a]	$RbNa_xCa_2Nb_3O_{10}$[b]
space group	$P4_2/ncm$ (No. 138)	$P4_2/ncm$ (No. 138)
a (Å)	5.4731(2)	5.4790(3)
c (Å)	29.0138(9)	28.8264(9)
Z	4	4
V (cm^3)	869.09(7)	865.35(9)
ρ (g/cm^3)	4.14	4.38
R_I (%)	5.94	7.05
R_{WP} (%)	6.72	13.31
R_E (%)	3.07	3.27

[a] Neutron diffraction data; wavelength of neutron = 1.8346 Å. [b] X-ray diffraction data.

interlayer charge density is enhanced by the sodium insertion into the rubidium layer. Such a contraction along the c axis is consistent with that found in other intercalated compounds.[12,20,22,24] The value of 0.43(3) for the sodium site occupancy corresponds to $x \sim 0.86$ per formula unit.

Structure Description. Table 3 summarizes the selected bond lengths and bond angles for β-$NaCa_2Nb_3O_{10}$ and $RbNa_xCa_2Nb_3O_{10}$. Their idealized structures are illustrated in Figures 4 and 5, respectively. As found in many $n = 3$ members of DJ- and RP-phases, outer $Nb1O_6$ octahedra of triple octahedral layers are strongly distorted while central $Nb2O_6$ octahedra are relatively regular. The average Nb2−O bond of $RbNa_xCa_2Nb_3O_{10}$ (~2.08 Å) is longer than that (~1.97 Å) of β-$NaCa_2Nb_3O_{10}$. This expansion of $Nb2O_6$ octahedra may arise as a result of partial reduction of Nb^V. An important feature in the structural data is that corner-shared NbO_6 octahedra are considerably tilted about the c axis in both compounds. The angle Nb1−O3−Nb2 decreases from 159.5(4)° of β-$NaCa_2Nb_3O_{10}$ to 152.2(8)° of $RbNa_x$-$Ca_2Nb_3O_{10}$, suggesting that the tilting degree is dependent on the nature of interlayer arrangement.

Of the most interest to us would be the structure of interlayer spaces. The arrangement of sodium atoms in the interlayer space of β-$NaCa_2Nb_3O_{10}$ is shown in Figure 6a. One O2−Na−O2 angle (~107°) between two Na−O2 (×2) bonds is close to the 109.5° angle for a perfect tetrahedron. On the other hand, the other O2−Na−O2 angle (~131°) between two Na−O2 (×1) bonds is largely deviated from 109.5°. This difference between two O2−Na−O2 angles would be induced by a significant tilting of $Nb1O_6$ octahedra about the c axis, and vice versa. A remarkable increase in the bond angle should then shift the sodium atom toward the next nearest neighboring oxygen atom O1 to form a Na−O1 bond of 2.83 Å. Such a 5-coordinated polyhedron for the sodium atom is quite different from the 9-coordination expected by Dion et al.[3a] The sodium atoms occupy one-half of these 5-coordinated sites in the interlayer spaces of β-$NaCa_2Nb_3O_{10}$. As shown in Figure 6b, the coordination environment around the sodium atom in $RbNa_x$-$Ca_2Nb_3O_{10}$ is somewhat similar to that in β-$NaCa_2$-Nb_3O_{10}. However, one O2−Na−O2 angle is decreased to ~104°, and the other is largely increased to ~154°. These changes in the O2−Na−O2 bond angle are accompanied by the more significant tilting of $Nb1O_6$ octahedra about the c axis of $RbNa_xCa_2Nb_3O_{10}$. Moreover, the enlarged O2−Na−O2 angle necessarily induces an increased displacement of the sodium atom from the ideal tetrahedral site toward the next nearest neighboring oxygen atom O1, which eventually results in a lengthening of the Na−O2 (×2) bonds (2.53 Å) and a shortening of the Na−O1 bond (2.29 Å).

The coordination environment around the rubidium atom is complicated. In the structure of parent $RbCa_2$-Nb_3O_{10}, the rubidium atom occupies the pseudocubic site which is located between triple octahedral slabs stacked in an eclipsed manner.[16] In contrast, a relative displacement of adjacent slabs toward a staggered conformation could not provide such an 8-coordinated site for the rubidium atom in $RbNa_xCa_2Nb_3O_{10}$. A 9-coordinated polyhedron is instead formed as found in the typical RP-phase $Rb_2La_2Nb_3O_{10}$.[29] Idealized interlayer structure for the RP-phases is shown in Figure 6c. Compared with those in the RP-phase, the coordination polyhedra for rubidium atoms are severely distorted in $RbNa_xCa_2Nb_3O_{10}$ (Figure 6b). Rubidium atoms occupy one-half of these sites so that the steric effect relative to sodium atoms is minimized. The large deviation of rubidium and sodium atoms from their regular 9-coodinated and tetrahedral sites in the interlayer spaces, coupled with the strong tilting of NbO_6 octahedra in the perovskite slabs, would be responsible for the highly unstable structure of $RbNa_xCa_2Nb_3O_{10}$.

A simple calculation based on the empirical expression $v_{ij} = \exp[(R_{ij} - d_{ij})/b]$, where R_{ij} and d_{ij} are the bond valence parameter and bond length, allows us to estimate valences in inorganic solids.[30] The calculated bond valences for Nb1 and Nb2 in β-$NaCa_2Nb_3O_{10}$ are 5.01 and 5.07, respectively, in excellent agreement with the

(29) Byeon, S.-H.; Nam, H.-J. *Chem. Mater.* **2000**, *12*, 1771.
(30) Brese, N. E.; O'Keeffe, M. *Acta Crystallogr., Sect. B* **1991**, *47*, 192.

Table 2. Atomic Positions and Isotropic Temperature Factors of β-$NaCa_2Nb_3O_{10}$ and $RbNa_xCa_2Nb_3O_{10}$

cmpd	atom	g^c	x	y	z	B(Å^2)
β-$NaCa_2Nb_3O_{10}$[a]	Na	0.5	0.24(2)	0.24(2)	0.2403(7)	2.6(6)
	Ca	1.0	0.4944(9)	0.0056(9)	0.0767(2)	0.76(8)
	Nb1	1.0	0.5064(7)	0.5064(7)	0.1452(2)	0.12(9)
	Nb2	1.0	0.0	0.0	0.0	0.14(9)
	O1	1.0	0.25	0.25	0.1426(5)	2.1(3)
	O2	1.0	0.0324(7)	0.4676(7)	0.2942(2)	0.30(8)
	O3	1.0	0.0459(8)	0.0459(8)	0.0645(3)	1.8(1)
	O4	1.0	0.75	0.75	0.1227(3)	0.23(9)
	O5	1.0	0.75	0.25	0.1307(2)	0.62(2)
	O6	0.5	0.192(2)	0.692(2)	0.0	1.8(4)
	O7	0.5	0.310(1)	0.190(1)	0.9845(5)	0.2(3)
$RbNa_xCa_2Nb_3O_{10}$[b]	Rb	0.5	0.048(4)	0.048(4)	0.2804(8)	1.0
	Na	0.43(3)	0.27(1)	0.27(1)	0.226(1)	1.0
	Ca	1.0	0.514(2)	−0.014(2)	0.0754(3)	1.1(2)
	Nb1	1.0	0.5001(9)	0.5001(9)	0.1456(1)	0.52(5)
	Nb2	1.0	0.0	0.0	0.0	0.93(7)
	O1	1.0	0.25	0.25	0.158(2)	1.0
	O2	1.0	0.033(5)	0.467(5)	0.2913(8)	1.0
	O3	1.0	0.067(4)	0.067(4)	0.0689(8)	1.0
	O4	1.0	0.75	0.75	0.120(2)	1.0
	O5	1.0	0.75	0.25	0.133(1)	1.0
	O6	0.5	0.159(6)	0.659(6)	0.0	1.0
	O7	0.5	0.321(8)	0.179(8)	0.975(2)	1.0

[a] Neutron diffraction data. [b] X-ray diffraction data. [c] Occupancy factor.

Table 3. Selected Bond Lengths (Å) and Bond Angles (deg) of β-$NaCa_2Nb_3O_{10}$ and $RbNa_xCa_2Nb_3O_{10}$

	β-$NaCa_2Nb_3O_{10}$	$RbNa_xCa_2Nb_3O_{10}$
	Bond Lengths	
Na−O2 (×2)	2.30(1)	2.53(2)
Na−O2 (×1)	2.36(8)	2.37(8)
Na−O2 (×1)	2.45(7)	2.43(8)
Na−O1 (×1)	2.83(2)	2.29(6)
Nb1−O2 (×1)	1.773(7)	1.84(3)
Nb1−O5 (×2)	1.981(2)	1.974(7)
Nb1−O1 (×1)	1.986(5)	1.97(1)
Nb1−O4 (×1)	1.996(6)	2.07(2)
Nb1−O3 (×1)	2.374(7)	2.27(2)
Nb2−O3 (×2)	1.905(7)	2.03(3)
Nb2−O6 (×2)	1.986(3)	2.05(2)
Nb2−O7 (×2)	2.040(4)	2.13(3)
	Bond Angles	
O1−Nb1−O4	158.8(5)	159(1)
O2−Nb1−O3	176.7(4)	175(1)
O2−Na−O2	107(1)	104(1)
	130.9(9)	154(2)
O1−Na−O2	66(2)	73(2)
	65(2)	81(2)
Nb1−O3−Nb2	159.5(4)	152.2(8)

theoretical valence of 5. In contrast, those in $RbNa_xCa_2Nb_3O_{10}$ are 4.78 and 3.93 for Nb1 and Nb2, respectively, suggesting that sodium incorporation leads to the reduction of Nb^V. The bond valence for Na in β-$NaCa_2Nb_3O_{10}$ and $RbNa_xCa_2Nb_3O_{10}$ is 0.97 and 0.95, respectively. This value is also close to the theoretical valence.

Magnetic Properties. Some reduced niobates with the mixed valence state have shown superconducting properties particularly in the low-temperature region. For instance, Li_xNbO_2 and Na_xNbO_2, whose hexagonal structure is composed of an edge-shared NbO_6 trigonal prism, exhibit superconductivity near 5 K.[31] According to the band calculation for the $n = 2$ member of the Ruddlesden−Popper series,[32] its electronic structure is sensitive to the off-plane movement of the equatorial oxygen atoms while the bending mode of the Nb−O−Nb bond along the c axis is almost irrelevant to the d-block bands. It was also suggested that chemical reduction in the $n = 3$ member leads to metallic conductivity because the conducting electrons in the central octahedral layer can be screened from the random potentials in the intervening alkali metal layer. Indeed, a superconducting transition was observed in the Li-intercalated $KCa_2Nb_3O_{10}$ below 2 K.[25]

The structure of $RbNa_xCa_2Nb_3O_{10}$ illustrated in Figure 5 shows that, relative to the severely distorted outer NbO_6 octahedra, the central NbO_2 layer does not show

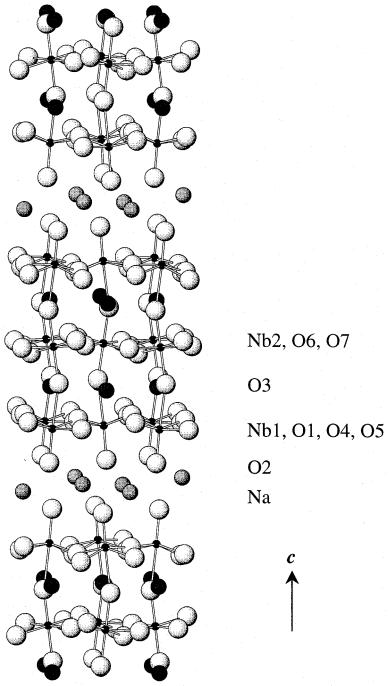

Figure 4. Idealized structure of β-$NaCa_2Nb_3O_{10}$ perpendicular to the c direction of the tetragonal unit cell. Only Nb−O bonds are represented by double lines (Na = shaded spheres, Ca = dark spheres, Nb = small black spheres, O = large white spheres).

(31) (a) Geselbracht, M. J.; Richardson, T. J.; Stacy, A. M. *Nature* **1990**, *345*, 324. (b) Rzeznik, M. A.; Geselbracht, M. J.; Thompson, M. S.; Stacy, A. M. *Angew. Chem., Int. Ed. Engl.* **1993**, *32*, 254.

(32) Rousseau, R.; Palacin, M. R.; Gomez-Romero, P.; Canadell, E. *Inorg. Chem.* **1996**, *35*, 1179.

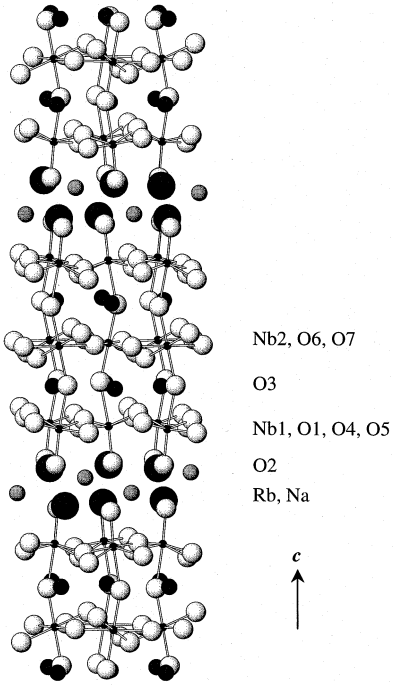

Figure 5. Idealized structure of $RbNa_xCa_2Nb_3O_{10}$ perpendicular to the *c* direction of the tetragonal unit cell. Only Nb−O bonds are represented by double lines (Rb = large dark spheres, Na = shaded spheres, Ca = small dark spheres, Nb = small black spheres, O = large white spheres).

any noticeable tilting even after the sodium insertion although a puckering of the equatorial O7 atoms is accompanied perpendicular to the ⟨110⟩ direction. We thus expected the black compound to show an interesting property as found in other reduced niobates. However, any indication of superconductivity was not found down to 5 K in our reduced niobate. As clearly seen in Figure 7, the magnetization measurement indicates a paramagnetic feature. The magnetization data are well fitted with a Curie−Weiss law, and the observed effective magnetic moment is ∼0.15 μ_B/mol. Although we have not measured the resistance with the sample because of the sensitivity to air, the black color implicates the metallic nature. A similar paramagnetic feature was observed in a potassium analogue, KNa_x-$Ca_2Nb_3O_{10}$; its structure has not been completely determined because of the poor crystallinity.

X-ray Absorption Near Edge Spectroscopy (XANES). In transition metal oxides with higher valent d-block metal ions, the first partially occupied or unoccupied state has a large weight of ligand 2p-character because of covalent mixing. The oxygen K-edge XANES features can be accordingly used to distinguish oxygen atoms under different bonding environments.[33,34] XANES spectra at O K-edge for β-$NaCa_2Nb_3O_{10}$, $RbCa_2Nb_3O_{10}$, and $RbNa_xCa_2Nb_3O_{10}$ are compared in Figure 8. The O K-edge spectra of β-$NaCa_2Nb_3O_{10}$ and $RbCa_2Nb_3O_{10}$ are quite similar in energy and shape to each other. This indicates that the electronic structure of oxygen is invariant regardless of distinctively different interlayer structures around sodium and rubidium ions, and thus,

(33) (a) de Groot, F. M. F. *J. Electron Spectrosc. Relat. Phenom.* **1994**, *67*, 529. (b) Chen, J. G. *Surf. Sci. Rep.* **1997**, *30*, 1.
(34) Glaser, T.; Hedman, B.; Hodgson, K. O.; Solomon, E. I. *Acc. Chem. Res.* **2000**, *33*, 859.

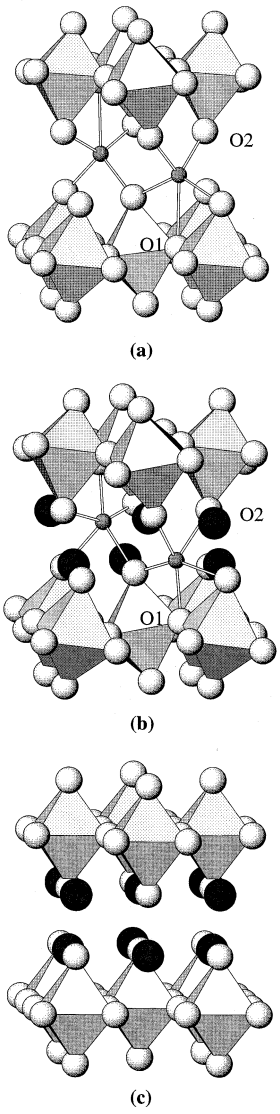

Figure 6. Schematic comparison of the interlayer arrangements of (a) β-$NaCa_2Nb_3O_{10}$, (b) $RbNa_xCa_2Nb_3O_{10}$, and (c) ideal Ruddlesden−Popper structure. Only Na−O bonds are represented by double lines. The octahedra represent the NbO_6 units (Rb = large dark spheres, Na = shaded spheres).

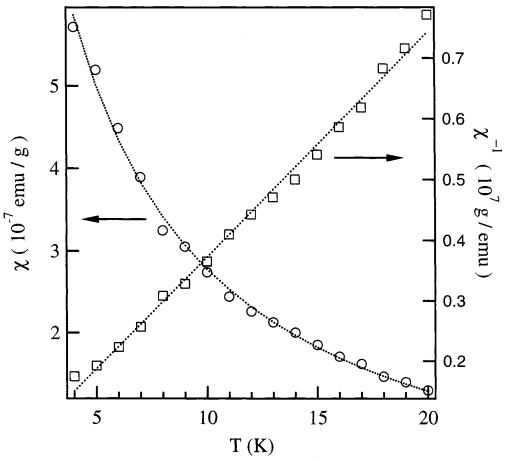

Figure 7. Temperature dependence of the magnetic susceptibility for $RbNa_xCa_2Nb_3O_{10}$ measured in the magnetic field of 100 G.

the alkali metal−oxygen bonds in the interlayer space have mainly ionic character. In both spectra of β-$NaCa_2$-

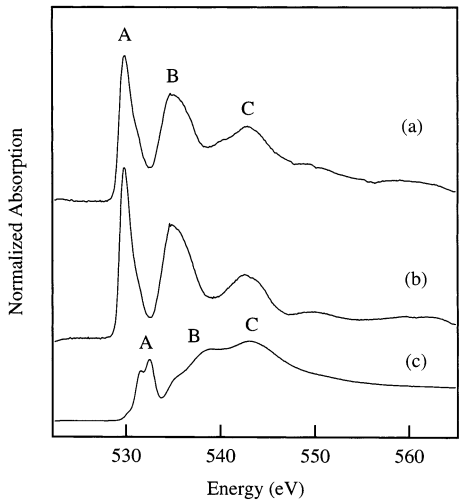

Figure 8. The O K-edge XANES spectra for (a) β-$NaCa_2Nb_3O_{10}$, (b) $RbCa_2Nb_3O_{10}$, and (c) $RbNa_xCa_2Nb_3O_{10}$.

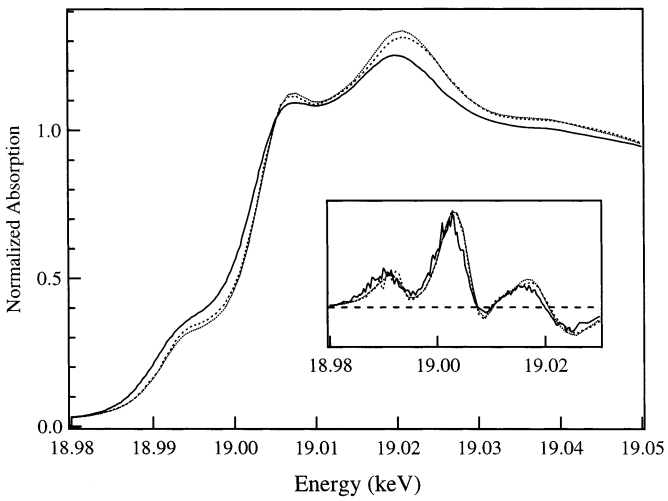

Figure 9. The Nb K-edge XANES spectra for β-$NaCa_2Nb_3O_{10}$ (dotted), $RbCa_2Nb_3O_{10}$ (dashed), and $RbNa_xCa_2Nb_3O_{10}$ (solid). Inset corresponds to the first derivatives.

Nb_3O_{10} and $RbCa_2Nb_3O_{10}$, the pre-edge peak (A) around 530 eV is assigned to the transition of an O 1s electron to O 2p-states in the d(t_{2g})-conduction band formed by niobium 4d- and oxygen 2p-orbitals. A shoulder at its high energy side would be attributed to an anisotropy of the d(t_{2g})-band due to nonequivalent oxygen atoms of the first coordination shell.[35] Peaks B and C are related to the transition to d(e_g) and 5s/5p of niobium ions hybridized with oxygen 2p-states, respectively. Especially, the energy difference of ~5 eV between the A and B peaks is well consistent with the splitting between the t_{2g} and e_g sub-bands for 4d-transition metal oxides, which is generally acceptable.

On the other hand, the shape of the O K-edge spectrum for $RbNa_xCa_2Nb_3O_{10}$ is in marked contrast to those of β-$NaCa_2Nb_3O_{10}$ and $RbCa_2Nb_3O_{10}$. Remarkable chemical shift and double-peaked structure of the pre-edge peak are also observed. The energy position of the pre-edge peak generally depends on the oxidation state or effective nuclear charge (Z_{eff}) of the metal ion, nature of ligand, and bond covalency.[34] Therefore, a reductive insertion of sodium could give rise to a shift of pre-edge position. Nevertheless, the observed pre-edge peak shift of ~2 eV appears too large to be induced by a small quantity of inserted sodium. Considering a decrease of the Nb1−O3−Nb2 angle and bond valence after the sodium insertion, it is conceivable that the weakened overlap of Nb 4d-states and O 2p-states leads to a higher Z_{eff} of the oxygen ion and a deeper binding energy of the O 1s core level in $RbNa_xCa_2Nb_3O_{10}$.[34,36] This should be responsible for a relatively large shift of the pre-edge to higher energy.

$RbNa_xCa_2Nb_3O_{10}$ also exhibits two resolved pre-edge features with an energy separation of ~1 eV. This energy separation is too small to be assigned as transitions to the t_{2g} and e_g bands, respectively. Instead, the splitting of the pre-edge might be attributed to the presence of strongly distorted outer $Nb1O_6$ octahedra and a less distorted inner $Nb2O_6$ one. Such a significant difference in distortion can induce a more anisotropic π^*(t_{2g})-band and/or a large difference in Z_{eff} of the ligands. The change of the rising edge is also understood in the same manner. That is, the anisotropy of the σ^*-(e_g)-band is more strongly influenced by ligand fields than that of π^*(t_{2g}). Two peaks at 535.5 and 538.5 eV are therefore ascribed to transitions to the σ^*(e_g)-band. In addition, the reduced intensity of the pre-edge peak would take into account the decreased statistical probability of a pre-edge transition due to the reduced d-hole numbers in the ground state as well as the decreasing of bond covalency due to more tilted sequence of NbO_6 octahedra.

Figure 9 displays the Nb K-edge XANES spectra of the three oxides studied. To show the spectral changes clearly, the first derivatives of the spectra are included as an inset. While β-$NaCa_2Nb_3O_{10}$ and $RbCa_2Nb_3O_{10}$ show almost the same spectra in shape and position as is in O K-edge spectra, sodium-inserted $RbNa_xCa_2Nb_3O_{10}$ exhibits a lower shift of the spectrum on the whole. This indicates that niobium ions are partially reduced by the insertion of additional sodium ions into the interlayer space, which is consistent with the fact expected from the bond valence calculation.

Acknowledgment. The authors thank Dr. M.-K. Lee and Dr. H. Shin for the soft X-ray absorption measurements for the O K-edge spectra. N.H.H. acknowledges the Creative Research Institute Program. This work was supported by Grant 2000-1-12200-004-1 from the Korea Science & Engineering Foundation.

CM020270B

(35) (a) Purans, J.; Kuzmin, A.; Parent, Ph.; Laffon, C. *Physica B* **1999**, *259−261*, 1157. (b) Purans, J.; Kuzmin, A.; Parent, Ph.; Laffon, C. *Electrochim. Acta* **2001**, *46*, 1973.

(36) Soldatov, A. B.; Povahzynaja, N. A.; Yalovega, G. E. *J. Phys. IV* **1997**, *7*, 512.